文章编号：1001－9014(2019)01－0015－06

DOI:10.11972/j.issn.1001－9014.2019.01.003

Design of a $TE_{34,10}$ mode cylindrical cavity for MW level gyrotron

MA Guo-Wu, HU Lin-Lin, ZHUO Ting-Ting, SUN Di-Min*, HUANG Yin-Hu, CHEN Hong-Bin, MENG Fan-Bao

(1. Institute of Applied Electronics, China Academy of Engineering Physics, Mianyang 621900, China)

Abstract: A cylindrical gyrotron cavity is designed and optimized with a high order mode $TE_{34,10-}$ to deliver an output power of megawatts level at 140 GHz. Analysis on mode competition indicates that the two adjacent modes $TE_{33,10-}$ and $TE_{31,11+}$ involve in competition and cause significant decreasing of output power of $TE_{34,10-}$. To suppress the competition hysteresis loops of $TE_{31,11+}$ and $TE_{33,10-}$ with $TE_{34,10-}$ are calculated, which indicates $TE_{34,10-}$ can inhibit growth of the other two modes with decreasing magnetic field from its low efficiency single mode oscillation zone, while it turned out just the opposite with increasing magnetic field due to the earlier oscillation of the competitors. Based on the results, a multimode time-dependent calculation including 42 modes is carried out with magnetic field dropping from 5.59 T to 5.51 T, the results show that mode competition is successfully suppressed, the operation mode $TE_{34,10-}$ realizes stable single mode oscillation with an output power of 0.96 MW and an electron efficiency of 36.7% at 140 GHz.

Key words: gyrotron, cylindrical cavities, mode competition

PACS: 84.40.Ik, 84.40.Fe, 07.57.Hm

用于MW级回旋管的$TE_{34,10}$模圆柱高频腔体设计

马国武，胡林林，卓婷婷，孙迪敏*，黄银虎，陈洪斌，孟凡宝

(中国工程物理研究院 应用电子学研究所,四川 绵阳 621900)

摘要:采用$TE_{34,10-}$模式开展了140 GHz兆瓦级圆柱回旋管腔体的设计和优化,并分析了工作模的模式竞争情况.由于两个邻近模式$TE_{33,10-}$和$TE_{31,11+}$的竞争$TE_{34,10-}$未能在高效率区稳定振荡,使得输出功率显著降低.为了抑制模式竞争计算了工作模和两个竞争模的滞回曲线,结果表明,$TE_{34,10-}$能够在磁场由其低功率振荡区下降时对竞争模形成抑制,而在磁场由低到高时则由于竞争模的率先起振反而被竞争模所抑制.基于此设计了由5.59 T下降至5.51 T的时变磁场曲线,在此磁场下开展了包含42个模式在内的多模时域计算,结果表明竞争模式被有效抑制,工作模在此磁场曲线下能够稳定获得0.96 MW的稳定输出功率,对应的电子效率为36.7%,频率为140 GHz.

关 键 词:回旋管;圆柱腔;模式竞争

中图分类号:O46　　**文献标识码**:A

Introduction

Gyrotrons can produce hundreds of kilowatts or higher continuous-wave (CW) power in millimeter wave and higher frequency bands[1,2]. They have important applications in magnetically confined fusion, such as plasma startup, heating, current driving and diagnostics[3-6]. To handle an output power of MW level, the operating mode order should be increased as high as possible to minimize the heat density on the cavity wall, but the mode competition deteriorates rapidly which restricts the further increasing of the mode order. In gyrotrons with cylindrical cavities which have realized MW level

Received date: 2018-04-14, **revised date**: 2018-05-23　　**收稿日期**:2018-04-14, **修回日期**:2018-05-23

Biography: MA Guo-Wu (1981-), male, Yuexi in Sichuan province, associate research fellow, master. Research area involves millimeter and terahertz vacuum electronics devices. E-mail: maguowu@caep.cn

* **Corresponding author**: E-mail: sundimin@tsinghua.org.cn

output power, high order modes such as $TE_{25,10}$[7], $TE_{28,8}$[8], $TE_{31,8}$[9] and $TE_{31,11}$[10] have been successfully used and achieved continuous operation time of hundreds of seconds, while higher order modes such as $TE_{31,12}$[11], $TE_{34,10}$[12], $TE_{32,18}$[13] and so on have been studied with numerical calculations or short-duration experiments to further reduce heat dissipation difficulty. However, stable operation of the higher order modes is always threatened by the mode competition. In the modes mentioned above, $TE_{34,10}$ is a promising candidate for MW level long pulse gyrotrons. Cavity designs with $TE_{34,10}$ have been carried out with PIC simulations in Ref. [12] and with a multimode time-dependent code named SELFT in Ref. [14], which show the $TE_{34,10}$ cavity have sufficient power capacity and acceptable efficiency for long pulse gyrotrons around 170 GHz.

In this paper, a cylindrical $TE_{34,10}$ cavity is designed with an in-house developed code GYO. We mainly focus on the possible competitors to the $TE_{34,10}$ mode and try to avoid the interference in the steady operation. A time-varying magnetic field is introduced into the starting process to realize single mode stable oscillation. The RF losses in the cavity is calculated, which is far less than the critical value. The structure of the article is organized as below: the first part briefly reviews the theoretical models used in GYO, which consists of LN-module for linear theoretical calculation, SSC-module for single-mode self-consistent theoretical calculations, and MTC-module for multimode time-dependent theoretical calculations. The second part presents the design of the cavity and suppression of competition modes. In the third part the loss power density on the cavity wall is obtained. Conclusion will be given in the end.

1 Theoretical model

The theoretical models used in GYO consist of the linear theory, the nonlinear self-consistent theory and the multimode time-dependent theory, which correspond to the LN module, SSC module and MTC module. The linear theory is always used to obtain the oscillation starting conditions, and the nonlinear self-consistent theory represents the stationary interaction of a single mode and the beam, which could be used to optimize the parameters. The multimode time-dependent theory can include several modes in the calculation and acquire multimode interaction state in time domain, which is helpful in analysis of mode competition.

One of the most important parameters derived from the linear theory is the threshold current, which could be described as[15]

$$-1/I_{st} = \left(\frac{QZ_0\eta}{8\gamma_0 c^2}\right)\left(\frac{\pi}{\lambda}\int_0^L |f(z)|^2 \mathrm{d}z\right)^{-1} \cdot \left(\frac{k_{mn}C_{mn}C_{mn}}{\beta_{z0}(s-1)!}\right)^2 \left(\frac{ck_{mn}\gamma_0\beta_{\perp 0}}{2\Omega_0}\right)^{2(s-1)} \cdot \left(s+\frac{1}{2}\frac{\omega\beta_{\perp 0}^2}{v_{z0}}\frac{\partial}{\partial\Delta_s}\right) \cdot \left|\int_0^L f(z)\mathrm{e}^{i\Delta_s z}\mathrm{d}z\right|^2 , \quad (1)$$

where

$$C_{mn} = \left[\sqrt{\pi(x_{mn}^2 - m^2)}J_m(x_{mn})\right]^{-1} , \quad (2)$$

$$G_{mn} = Jm \mp s(k_{mn}R_c) , \quad (3)$$

where $f = |f|\exp(-i\psi(z))$ is field profile function, Q is quality factor of the cavity, Z_0 is wave impedance in vacuum, η is charge-mass ratio, s is the harmonic number, $m - +s$ corresponds to the case of azimuthal co-rotation and counter-rotation of the wave and the electron, $\beta_{\perp 0}$ is transverse velocity and β_{z0} is axial velocity of electrons normalized by light speed c respectively, $k_\perp$ is transverse wave number, R_e is injection radius of the beam, $\Delta_s(z)$ is the mode detuning parameter given by

$$\Delta_s(z) = \frac{\omega}{v_{z0}}\left(1 - \frac{s\Omega_0}{\omega\gamma_0}\right) , \quad (4)$$

where ω is frequency of wave and $\Omega_0 = eB/m_0$ is non-relativistic cyclotron frequency of electron. The coupling coefficient represents the coupling strength between electron beam and specific mode, and could be described by[16]

$$C_{BF} = \frac{J_{m\pm s}^2(k_\perp R_e)}{(x_{mn}^2 - m^2)J_m^2(x_{mn})} . \quad (5)$$

Equation (5) indicates the strongest coupling occurs at the first maximum of $J_{m-s}(k_\perp R_e)$, which is also the first zero of $J'_{m-s}(k_\perp R_e)$.

The nonlinear self-consistent theory is composed of the adiabatic equation for electron motion and the wave equation for the RF field profile function, which can be expressed respectively as[17]

$$[\mathrm{d}/\mathrm{d}\ell + (i\gamma/\gamma_0)(1/s - \bar{\Omega}_0/\gamma\bar{\omega})]P = -(1/2\bar{\omega})(\gamma/\gamma_0)(\bar{k}_{mn}/\bar{\Omega}_0)^{s-1}(J_{m-s}(\bar{k}_{mn}\bar{R}_0)/\bar{r}_w)F(P^{s-1})^* , \quad (6)$$

and

$$[\mathrm{d}^2/\mathrm{d}\ell^2 + \beta_{z0}^2(1 - \bar{k}_{mn}^2/\bar{\omega}^2)]F = -(i\mu\eta/c)\beta_{z0}(I_0/\gamma_0\bar{\omega})[x_{mn}C_{mn}/2^{s-1}(s-1)!]^2(\bar{k}_{mn}/\bar{\Omega}_0)^{s-1} \times [J_{m-s}(\bar{k}_{mn}\bar{R}_0)/\bar{r}_w](1/2\pi)\int_0^{2\pi}\mathrm{d}\Lambda_0 P^s , \quad (7)$$

where $P = \bar{u}_t\exp(-i\Lambda)$ is normalized momentum variable, $\bar{u}_t = \gamma v_t/c$ is the normalized transverse momentum, $\beta_{z0} = v_{z0}/c$ is normalized initial axial velocity, $\Lambda = (\omega/s - \Omega)\tau + \omega/st_0 - \phi$ is slow time phase variable, $\bar{\Omega} = \Omega r_{w0}/c = \Omega_0 r_{w0}/\gamma_0 c$ is normalized cyclotron frequency of the electron, r_{w0} is an arbitrary radius for normalization, t_0 is the moment when electrons enter the cavity, $\tau = t - t_0$, φ is the polar angle of guiding center, $F = C_{mn}X_{mn}\eta f/c^2 2^{s-1}!$ is normalized field profile function, $C_{mn} = \{\sqrt{[\pi(x_{mn}^2 - m^2)]J_m(x_{mn})}\}^{-1}$ is a normalization constant, $r_w = r_w/r_{w0}$ is normalized wave guide radius, $\bar{R}_e = R_e/r_w$ is normalized injection radius, $\bar{k}_{mn} = k_{mn}/r_{w0}$ is normalized transverse wave number, $\ell = \omega z/v_{z0} = \omega(t - t_0)$ is normalized z coordinate of the electron.

The multimode time-dependent theory could be derived from the nonlinear self-consistent theory based on the fact that characteristic rise time of fields in the resonator is much longer than the electron transit time in the cavity as well as the wave period, which are given by[18]

$$\frac{\mathrm{d}a_n}{\mathrm{d}t} + \frac{\omega_0 a_n}{2Q_n} = \frac{-1}{2\varepsilon_0}\mathrm{Im}\Re_n(t) , \quad (8)$$

and

$$\frac{d\psi_n}{dt} + \omega_0 - \omega_n = \frac{1}{2\varepsilon_0 a_n}\mathrm{Re}\Re_n(t) \quad , \quad (9)$$

where $a_n(t)$ is amplitude and ψ_n is phase of the field, ω_n is a nearby reference frequency, ε_0 is permittivity of free space, $\Re_n(t) = i\int_V \mathrm{d}a\mathrm{d}zf(z)\vec{e}_n^* \cdot \vec{J}_\omega e^{i\psi}/W$ is the complex slow-time-scale component of the electron-beam polarization, $\vec{e}_n^*$ is the waveguide transverse-mode vector function, $\vec{J}_\omega = \int_0^{2\pi} d(\omega_0 t)\vec{J}_t e^{i\omega_0 t}$ is the rf current density, $\vec{J}_t$ is the transverse current density of the beam, $W = \int_0^L \mathrm{d}z \mid f(z) \mid^2$. The definition of other variables in (8) and (9) is the same as in (6) and (7), except the subscript identifies the mode n.

2　Design of the cavity and realization of single-mode steady operation

A simple three-segment structure including down taper, uniform section and up taper is adopted in the cavity. The length of the uniform section is expressed as L and the radius of the uniform section is R_0. R_0 is set as 25.45 mm according to the cutoff frequency of the waveguide. The cavity structure and field distribution under different L are shown in Fig. 1(a). The resonant frequency and the Q-factor of the cavity are shown in Fig. 1(b).

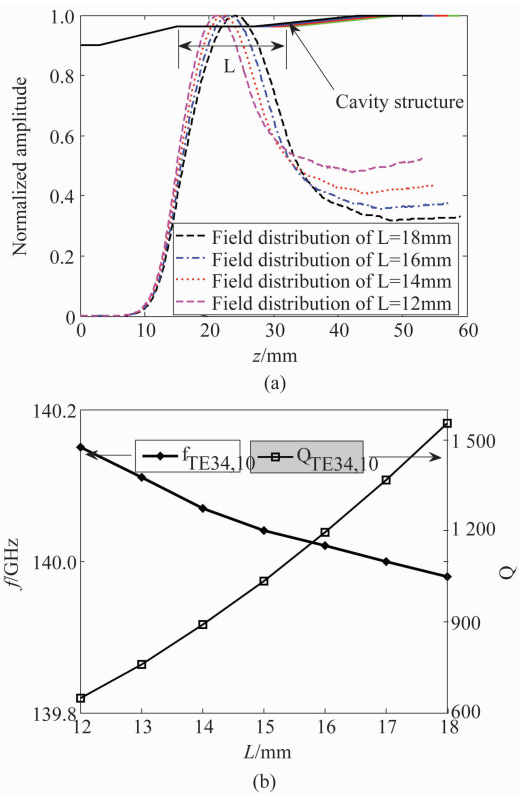

Fig. 1　(a) Cavity structure and field distribution, (b) resonant frequency and Q factor of the cavity

图 1　(a)腔体结构和场分布,(b)谐振频率和 Q 值

We choose co-rotation of the wave and the beam for better beam-wave interaction which means the operation mode is $TE_{34,10-}$. With beam voltage 75 kV, beam current 35 A, pitch factor 1.5 and injection radius 12.16 mm, the output power of the cavity is calculated with SSC module, the results are shown in Fig. 2. As shown in the figure, the output power rises with L, but the growth rate slows down when it reaches 16 mm. Although longer cavity length can increase output power slightly, it will bring the risk of deterioration of mode competition, so we choose L to be 16 mm, the maximum output power could reach 1.1 MW at magnetic field of 5.52 T with an efficiency of 41.9%.

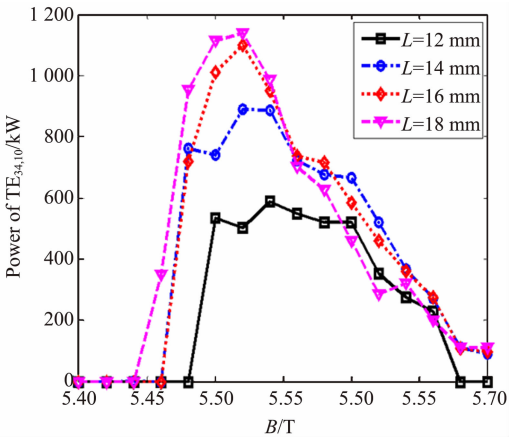

Fig. 2　Output power versus magnetic field under different L calculated by SSC module

图 2　采用 SSC 模块计算的不同 L 下的输出功率与磁场的关系

Now we consider the modes which might participate in competition with operation mode $TE_{34,10}$. The coupling coefficients and corresponding eigenvalues of the nearby modes are plotted in Fig. 3(a), in which $TE_{31,11+}$ and $TE_{33,10-}$ have the coupling coefficient similar to $TE_{34,10-}$. The threshold currents of the modes are plotted in Fig. 3(b), we can see that many of the neighbor modes have starting current below 35 A and therefore are capable of oscillating, so the process of starting oscillation is also a process of competition among these modes.

The MTC module is used to study the starting process of the oscillation, 13 modes thought to be most dangerous are included according to Fig. 3(a) and fixed static magnetic field is adopted. The results are counted in Fig. 4(a), which shows that $TE_{34,10-}$ can only achieve stable oscillation between 5.57 T and 5.68 T but fails at magnetic field between 5.44 T and 5.56 T where $TE_{33,10-}$ or $TE_{31,11+}$ dominates the oscillation. The results of SSC calculation of the three modes are also given in Fig. 4(a) which expect an output power of 1.1 MW for $TE_{34,10-}$, but only 664 kW could be achieved according to the MTC calculation due to the competition of $TE_{33,10-}$ and $TE_{31,11+}$.

Fig. 4(b) shows the time behavior of the modes with a fixed magnetic field of 5.55 T, the initial power of each mode is set to be 0.1 kW. The power of $TE_{28,12-}$,

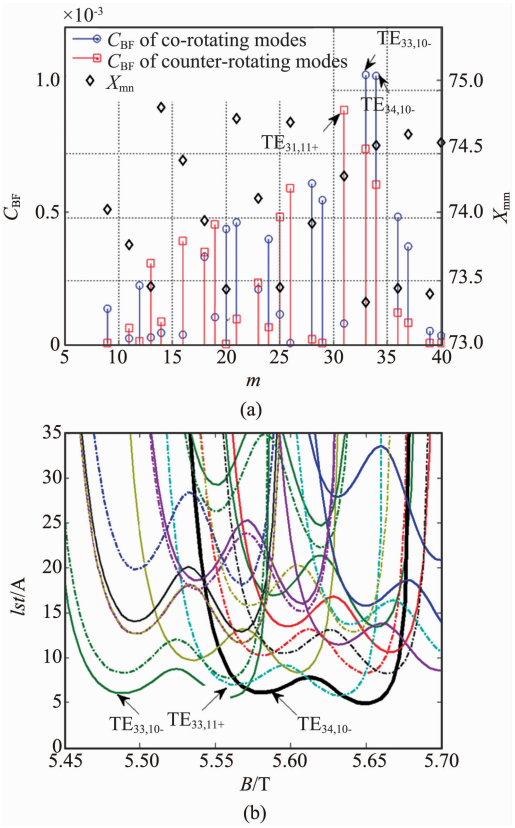

Fig. 3 (a) Coupling coefficient of co-rotating modes (blue circles) and counter-rotating modes (red squares), together with the eigenvalues of the modes (black diamonds). (b) Threshold current curves of co-rotating modes (solid lines) and counter-rotating modes (dashed lines) whose eigenvalues are close to $TE_{34,10}$

图3 (a)各模式的耦合系数,包括同向旋转模式(蓝色圆圈)和反向旋转模式(红色方块),同时给出了模式的本征值(黑色菱形);(b)本征值在 $TE_{34,10}$ 附近的模式的起振电流,包括同向旋转模式(实线)和反向旋转模式(虚线)

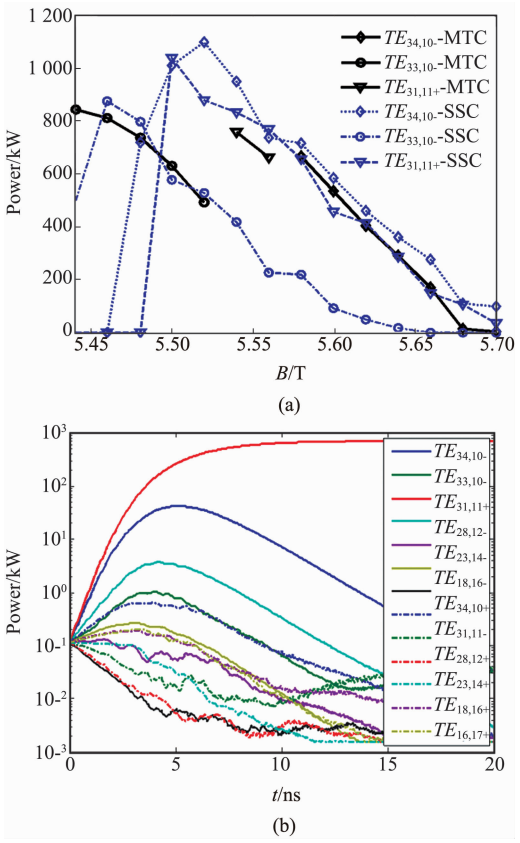

Fig. 4 (a) Output power versus magnetic field calculated by SSC (blue dashed lines) and MTC (black solid lines). (b) Output power of each mode versus time at B = 5.56 T

图4 (a)SSC 模块(蓝色虚线)和 MTC 模块(黑色实线)计算的输出功率与磁场的关系;(b)B = 5.56 T 时各模式输出功率与时间的关系

$TE_{31,11+}$, $TE_{33,10-}$, $TE_{34,10-}$ and $TE_{34,10+}$ grow together in the beginning, while $TE_{31,11+}$ have the maximal growth. The output power of the other modes reaches the inflection point at about 5 ns, after the output power of $TE_{31,11+}$ grows to saturation, all the other modes are suppressed and the system is dominated by $TE_{31,11+}$, the expected operation mode $TE_{34,10-}$ fails to achieve stationary oscillation finally.

The magnetic field we use in the calculations above is a fixed one, which doesn't seem to achieve an efficient operation state for $TE_{34,10-}$ mode. From Fig. 4(a) we can see that $TE_{34,10-}$ can obtain stable oscillation at magnetic field between 5.57 T and 5.68 T, due to the inhibition effect of the preset field on the other mode, a time-varying magnetic field which decreases after the operation mode achieving stable oscillation might be helpful to improve the efficiency. To verify the feasibility of the method, it is necessary to obtain the hysteresis curves of $TE_{31,11+}$ and $TE_{33,10-}$ with $TE_{34,10-}$ first. The scanning range of the magnetic field is chosen to be 5.45 T ~ 5.59 T, the scanning process is that the magnetic field decreases from 5.59 T to 5.45 T at a uniform speed in 500 ns, then maintains 5.45 T for 100 ns, and then rises to 5.59 T again in 500 ns. The calculated hysteresis loop of $TE_{33,10-}$ and $TE_{34,10-}$ is shown in Fig. 5(a). As shown in the Fig. 5(a), $TE_{34,10-}$ starts oscillation first at $B = 5.59$ T, while $TE_{33,10-}$ damps rapidly. In the process of magnetic field falling from 5.59 T, $TE_{34,10-}$ remains dominant and its output power increases gradually and reaches the maximum at about 5.5 T. After that, the output power of $TE_{34,10-}$ begins to decrease as the magnetic field decreases. When the magnetic field reaches 5.485 T, the dominant mode is switched from $TE_{34,10-}$ to $TE_{33,10-}$. The output power of $TE_{34,10-}$ decreases rapidly while $TE_{33,10-}$ rises to the peak. As the magnetic field continues to decrease, the power of $TE_{33,10-}$ is still rising until it reaches 5.45 T. After the retention time of 100 ns, the magnetic field begins to increase, $TE_{33,10-}$ remains dominant until the magnetic field increases to 5.58 T where the oscillation mode is switched from $TE_{33,10-}$ to $TE_{34,10-}$ again. In the magnetic field area between 5.485 T and 5.58 T, both modes can achieve steady single-mode oscillation, the dominant mode is determined by the changing direction of the magnetic field. Similar conclusion can also be obtained from

the hysteresis loop between $TE_{31,11+}$ and $TE_{34,10-}$ as shown in Fig. 5(b). In fact, the above phenomenon is caused by the inhibition effect of the mode which obtains a certain oscillation amplitude first on the other modes. So, to realize a high-power output of $TE_{34,10-}$, we can start at arbitrary magnetic field between 5.57 T and 5.68 T where $TE_{34,10-}$ can retain single-mode steady oscillation, and change the magnetic field to a more efficient point after the expected mode is excited.

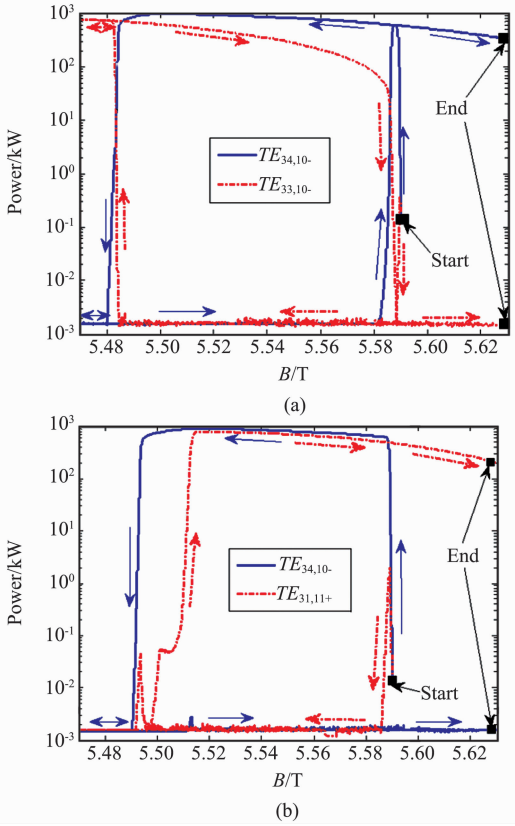

Fig. 5　(a) Hysteresis loop between $TE_{34,10-}$ and $TE_{33,10-}$, (b) Hysteresis loop between $TE_{34,10-}$ and $TE_{31,11+}$. The magnetic field varies as: decreasing from 5.59 T to 5.45 T in 500 ns, then maintaining 5.45 T for 100 ns, and then rising to 5.59 T again in 500 ns

图 5　(a) $TE_{34,10-}$ 和 $TE_{33,10-}$ 的滞回曲线; (b) $TE_{34,10-}$ and $TE_{31,11+}$ 的滞回曲线. 其中磁场的变化过程为: 在 500 ns 内由 5.59 T 下降至 5.45 T, 并在 5.45 T 维持 100 ns, 然后再次在 500 ns 内上升至 5.59 T

The dependence of magnetic field on time we use finally is shown in Fig. 6, which also contains the corresponding MTC calculation results including 42 neighbor co-rotating and counter-rotating modes. From Fig. 6 we can see the magnetic field maintains 5.59 T for 5 ns, during which the output power of $TE_{34,10-}$ increases to more than 100 kW, while most of the other modes have negative growth rate except several modes growing with it and reaching their inflection point at about 4 ns. After that the magnetic field starts to decrease, and the power of $TE_{34,10-}$ continues to grow. The system achieves single mode steady operation of $TE_{34,10-}$ at last with an output

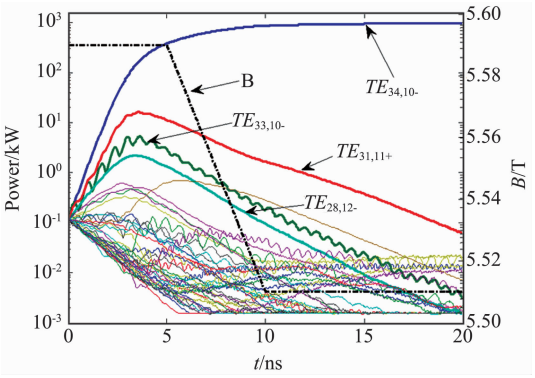

Fig. 6　MTC calculation results including 42 modes with time-varying magnetic field

图 6　在时变磁场下包含 42 个模式在内的 MTC 计算的结果

power of 964 kW and an efficiency of 36.7% at magnetic field of 5.51 T. The mode competition is successfully suppressed, and the power of all other modes is far less than 1 kW at the end of the calculation. The output power of $TE_{34,10-}$ is still smaller than the maximum 1.1 MW obtained by SSC calculation, which may be caused by the influence of the other modes with small amplitudes on the interaction between the operation mode and the beam.

3　Ohmic wall loss

In the interaction cavity, some amount of RF power is lost due to the ohmic wall loss, which would heat the cavity and elevate the temperature of the wall. So cooling system is needed to keep the temperature within a certain range. To ensure feasible operation of the gyrotron, a general limitation is set for the wall loading as 2 kW/cm^2 for CW operation[19]. The ohmic wall loss can be calculated as below[20]

$$\frac{\mathrm{d}P_{loss}}{\mathrm{d}A} \simeq \frac{\delta}{4\pi\mu_0\omega}\left[\frac{1}{x_{mn}^2 - m^2}\right]\left(k_{mn}^4 \mid f \mid^2 + \frac{m^2}{r_w^2}\left|\frac{\mathrm{d}f}{\mathrm{d}z}\right|^2\right), \quad (10)$$

where $\delta = \sqrt{2/\mu_0\omega\sigma}$ is the skin depth, μ_0 is the permittivity, σ is the electrical conductivity. The other parameters are the same as before.

The wall loading of the cavity is calculated as in Fig. 7, the peak loss power density is about 0.67 kW/cm^2 with an output power of about 1 MW, which is far less than the critical value. It makes the heat dissipation easier and is helpful to improve the stability and reliability of the gyrotron.

4　Conclusions

A cavity operating at $TE_{34,10-}$ is designed in the article. According to the analysis of eigenvalues and coupling coefficients of the neighbor modes, $TE_{33,10-}$ and $TE_{31,11+}$ are more dangerous to the operation mode than the else, which is verified by MTC calculations. Using the time-varying magnetic field method the mode compe-

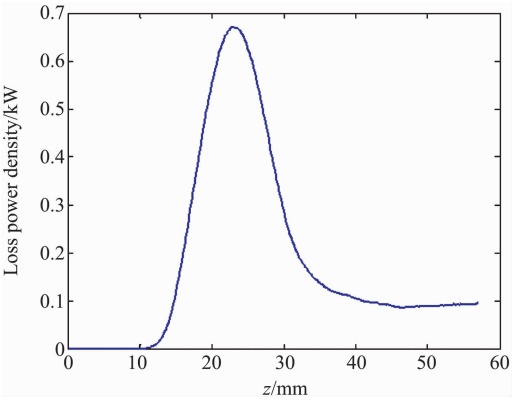

Fig. 7 Distribution of loss power density on the cavity wall
图 7 腔壁损耗功率密度的分布

tition is suppressed and single-mode steady operation with an output power of 964 kW at 140 GHz is achieved. The peak ohmic wall loading of the cavity is only 0.67 kW/cm^2, which is beneficial for cooling system design and achieving stable CW operation. Besides, according to our analysis, as long as we can make the expected mode start first, competitive inhibition can be achieved, so adjustment methods based on other parameters may be also feasible, such as the beam voltage, pitch factor, etc.

References

[1] Nusinovich G S, Thumm M K A, Petelin M I. The Gyrotron at 50: Historical Overview[J]. *Journal of Infrared Millimeter & Terahertz Waves*, 2014, **35**(4):325-381.

[2] FU Wen-Jie, GUAN Xiao-Tong, CHEN Chi, et al. A 220GHz high-power coaxial cavity gyrotron[J]. *J. Infrared Millim. Waves*, (傅文杰, 关晓通, 陈驰, 等. 220 GHz 高功率同轴谐振腔回旋管. **红外与毫米波学报**) 2014, **33**(6):613-618.

[3] Gaponov A V, Flyagin V A, Goldenberg A L, et al. Powerful millimetre-wave gyrotrons[J]. *International Journal of Electronics*, 1981, **51**(4):277-302.

[4] Thumm M. Progress on Gyrotrons for ITER and Future Thermonuclear Fusion Reactors[J]. *IEEE Transactions on Plasma Science*, 2011, **39**(4):971-979.

[5] Litvak A, Sakamoto K, Thumm M. Innovation on high-power long-pulse gyrotrons[J]. *Plasma Physics & Controlled Fusion*, 2011, **53**(12):124002.

[6] Poli E, Tardini G, Zohm H, et al. Electron-cyclotron-current-drive efficiency in DEMO plasmas[J]. *Nuclear Fusion*, 2013, **53**(1):013011.

[7] Litvak A G, Denisov G G, Myasnikov V E, et al. Recent Development Results in Russia of Megawatt Power Gyrotrons for Plasma Fusion Installations[C]// *EDP Sciences*, 2012:04003.

[8] Thumm M, Alberti S, Arnold A, et al. EU Megawatt-Class 140-GHz CW Gyrotron[J]. *IEEE Transactions on Plasma Science*, 2007, **35**(2):143-153.

[9] Sakamoto K, Kasugai A, Kajiwara K, et al. Progress of high power 170 GHz gyrotron in JAEA[J]. *Nuclear Fusion*, 2009, **49**(9):095019.

[10] Ikeda R, Oda Y, Kobayashi T, et al. Development of 170 GHz, 1 MW gyrotron with high-order TE 31,11, mode oscillation for ITER EC system[J]. *Fusion Engineering & Design*, 2018, **128**:23-27.

[11] Kajiwara K, Oda Y, Takahashi K, et al. Design and Operation of TE 31,12 High Power Gyrotron[J]. *Fusion Science & Technology*, 2013, **63**(1T):35-39.

[12] Kumar A, Kumar N, Singh U, et al. Towards a 1 MW, 170 GHz gyrotron design for fusion application[J]. *Infrared Physics & Technology*, 2013, **57**(3):1-7.

[13] Sakamoto K, Kariya T, Oda Y, et al. Study of sub-terahertz high power gyrotron for ECH&CD system of DEMO[C]// *IEEE International Conference on Plasma Sciences. IEEE*, 2015:1-1.

[14] Kern S, Borie E, Illy S, et al. Theoretical study of 174 GHz operation of the W7-X 1 MW, 140 GHz gyrotron[C]// *International Conference on Infrared, Millimeter and Terahertz Waves*, California Institute of Technology Pasadena, California, USA, 2008:1-2.

[15] Borie E, Jodicke B. Comments on the linear theory of the gyrotron [J]. *IEEE Transactions on Plasma Science*, 2002, **16**(2):116-121.

[16] Nusinovich G S. *Introduction to the Physics of Gyrotrons*[M]. Baltimore, MD: John Hopkins University Press, 2004, 62.

[17] Fliflet A W, Read M E, Chu K R, et al. A self-consistent field theory for gyrotron oscillators: application to a low Q gyromonotron[J]. *International Journal of Electronics*, 1982, **53**(6):505-521.

[18] Fliflet A W, Lee R C, Gold S H, et al. Time-dependent multimode simulation of gyrotron oscillators[J]. Physical Review A, 1991, **43**(11):6166-6176.

[19] Gantenbein G, Borie E, Dumbrajs O, *et al*. Design of a high order volume mode cavity for a 1 MW/140GHz gyrotron[J]. *International Journal of Electronics*, 1995, **78**(4):771-787.

[20] Jackson, J. D. *Classical Electrodynamics*[M]. New York: John Wiley & sons, Inc., 1962, 36.